

Elastic-plastic fracture of functionally graded circular shafts in torsion

Victor I. Rizov*

*Department of Technical Mechanics, University of Architecture, Civil Engineering and Geodesy,
1 Chr. Smirnensky blvd., 1046 - Sofia, Bulgaria*

(Received October 15, 2016, Revised November 28, 2016, Accepted February 8, 2017)

Abstract. Analytical investigations were performed of a longitudinal crack representing a cylindrical surface in circular shafts loaded in torsion with taking into account the non-linear material behavior. Both functionally graded and multilayered shafts were analyzed. It was assumed that the material is functionally graded in radial direction. The mechanical behavior of shafts was modeled by using non-linear constitutive relations between the shear stresses and shear strains. The fracture was studied in terms of the strain energy release rate. Within the framework of small strain approach, the strain energy release rate was derived in a function of the torsion moments in the cross-sections ahead and behind the crack front. The analytical approach developed was applied to study the fracture in a clamped circular shaft. In order to verify the solution derived, the strain energy release rate was determined also by considering the shaft complimentary strain energy. The effects were evaluated of material properties, crack location and material non-linearity on the fracture behavior. The results obtained can be applied for optimization of the shafts structure with respect to the fracture performance. It was shown that the approach developed in the present paper is very useful for studying the longitudinal fracture in circular shafts in torsion with considering the material non-linearity.

Keywords: functionally graded material; torsion; fracture; elastic-plastic behavior; analytical solution

1. Introduction

Recently, the application of functionally graded materials in structures that are subjected to non-uniform service requirements has increased rapidly (Gasik 2010, Nemat-Allal *et al.* 2011, Bohidar *et al.* 2014, Abdelhak *et al.* 2015, Daouadji and Adim 2016, Daouadji *et al.* 2016). This is due mainly to the fact that functionally graded materials allow for spatial optimization of composition and properties in one or more directions during manufacturing. In this way, novel materials that have remarkable advantages over the traditional structural materials can be manufactured. Bending of functionally graded plates and beams has been analyzed recently by Ait Yahia *et al.* 2015, Belabed *et al.* 2014, Bellifa *et al.* 2016, Bennoun *et al.* 2016, Bouderra *et al.* 2013, Bourada *et al.* 2015, Bourada *et al.* 2016, Bousahla *et al.* 2014, Hadji *et al.* 2016, Hamidi *et al.* 2015, Mahi *et al.* 2015). The study of fracture behavior of functionally graded materials plays

*Corresponding author, Professor, E-mail: v_rizov_fhe@uacg.bg

an important role in the design of structures composed by these novel materials (Pei and Asaro 1997, Tilbrook *et al.* 2005, Carpinteri and Pugno 2006, Ivanov and Draganov 2014, Ivanov *et al.* 2016, Upadhyay and Simha 2007, Zhang *et al.* 2013).

Studies of fracture in functionally graded materials by applying the methods of linear-elastic fracture mechanics have been reviewed by Tilbrook *et al.* (2005). Analyses of stress intensity factors have been presented. Cracks oriented parallel and perpendicular to the gradient direction have been considered. Fatigue fracture behavior under cyclic loading has also been studied.

Cracks in functionally graded linear-elastic materials have been investigated by Carpinteri and Pugno (2006). Fracture behavior of functionally graded plate in tension and beam under three-point bending has been analyzed. Stress intensity factors have been evaluated. A method for predicting the strength of structures composed by functionally graded materials has been developed.

Equivalent homogeneous beams of variable depth have been suggested for evaluation of the stress intensity factor in cracked functionally graded linear-elastic beams under three-point bending (Upadhyay and Simha 2007). The compliance method has been applied. It has been found that the equivalent beam with cubic variation in height captures the compliance characteristics of functionally graded beams. It has been shown that the method developed is particularly suitable for analysis of cracked beams loaded by concentrated forces.

Multilayered materials have many useful properties, such as light weight and high strength which facilitate an extensive use of these materials in various engineering applications including load bearing structures. Interface fracture between layers is the primary concern with multilayered structures. Initiation and growth of interface cracks can reduce significantly the stiffness and strength of multilayered materials. Therefore, the interface fracture continues to attract the interest of researchers (Jiao *et al.* 1998, Yeung *et al.* 2000, Guadette *et al.* 2001, Markov and Dinev 2005, Tuan and Wei 2009, Szekrenyes 2010, Szekrenyes and Vicente 2012, Her and Su 2015).

Interface cracks have been studied in linear-elastic multilayered beams under four-point bending (Tuan and Wei 2009). Fracture behavior has been analyzed in terms of strain energy release rate by using the conventional beam theory. The beams investigated can have an arbitrary number of layers and cracks can be located at any interface.

Interfacial fracture has been analyzed in multilayered beam structures by applying the methods of linear-elastic fracture mechanics (Her and Su 2015). An analytical solution has been derived for strain energy release rate in a function of material properties and layer thicknesses by using the crack tip cross-sectional bending moment.

The literature review indicates that fracture in functionally graded and multilayered structures has been studied usually assuming linear-elastic material behavior. However, a realistic appraisal of the potential for crack growth should include the effects of material non-linearity. Therefore, the main purpose of present paper was to develop the general analysis of a longitudinal crack representing a cylindrical surface in functionally graded and multilayered circular shafts in torsion with considering the non-linear behavior of material (the present paper was motivated also by the fact that calculation of structural members in torsion takes an important place in the design of machines and engineering equipments). The fracture was analyzed in terms of strain energy release rate by using the torsion moments in cross-sections ahead and behind the crack front. The influence of crack location and material properties on the non-linear fracture was evaluated. It should be mentioned that the present paper deals with analytical solutions, since they are very suitable for parametric investigations in contrast to the finite element method which suffers from relatively limited abilities in parametric studies.

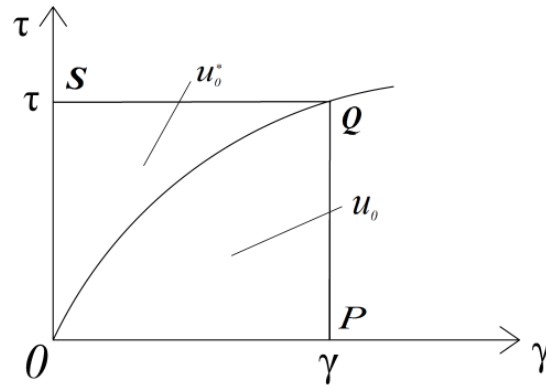


Fig. 1 Non-linear stress-strain curve with strain energy density, u_0 , and complimentary strain energy density, u_0^*

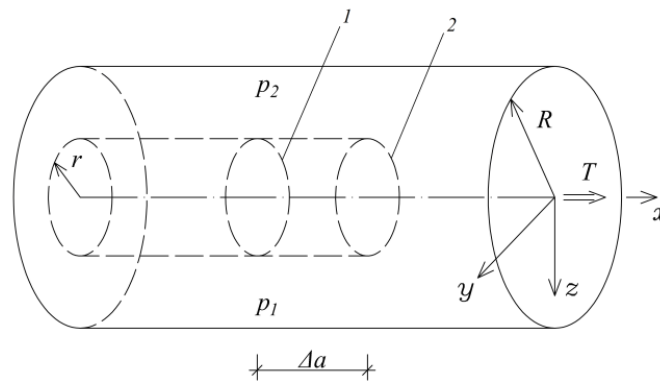


Fig. 2 Portion of a circular shaft with the crack front (1-crack front position before the increase of crack, 2-crack front position after the increase of crack). The longitudinal crack represents a cylindrical surface of radius r

2. Elastic-plastic fracture analysis

The present paper deals with elastic-plastic analysis of a longitudinal crack in circular shafts loaded in torsion. The longitudinal crack represents a cylindrical surface (the crack front is a circle of radius r). Thus, the internal crack arm is a solid shaft with circular cross-section of radius r . The external crack arm is a shaft with ring-shaped cross-section with internal radius r and external radius R . The loading consists of concentrated and/or distributed torsion moments applied on the shaft. The internal crack arm can also be loaded in torsion (for instance, by a torsion moment applied on the free end of internal crack arm).

It was assumed that the mechanical response of shaft considered can be modeled by a non-linear stress-strain curve (Fig. 1). The non-linear stress-strain relation was written in the general form

$$\tau = \tau(\gamma), \tag{1}$$

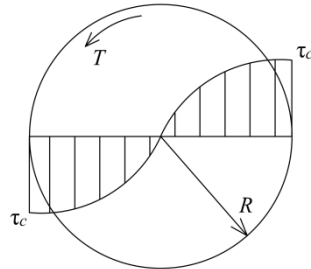


Fig. 3 Distribution of shear stresses in shaft cross-section p_1p_2 (refer to Fig. 2) before the increase of crack

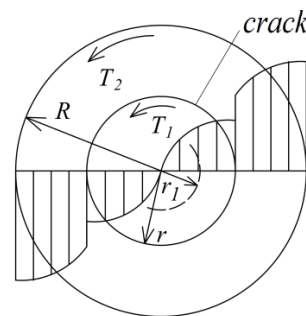


Fig. 4 Distribution of shear stresses in shaft cross-section p_1p_2 (refer to Fig. 2) after the increase of crack

Where τ is the shear stress, γ is the shear strain.

First, a circular shaft made by functionally graded material was considered (it was assumed that the material is functionally graded in radial direction). A shaft portion with the crack front is shown schematically in Fig. 2. The cross-sectional torsion moment ahead of the crack front is T . A crack increase by length Δa would lead to change of the shear stresses distribution in the shaft cross-section, p_1p_2 , (Fig. 2). Thus the distribution shown in Fig. 3 changes to that reported in Fig. 4.

The main goal of present study was to develop the general analysis of crack problem shown in Fig. 2 with taking into account the material non-linearity. The analysis was performed in terms of the strain energy release rate. In principle, the fracture analysis developed in the present paper can be applied for non-linear elastic materials.

Besides, the analysis is applicable also for elastic-plastic materials, if the external load magnitude increases only, i.e., if the shaft undergoes active deformation (Chakrabarty 2006). Also, the present study is based on the small strain assumption (it should be noted that this assumption has been frequently used in fracture analyses of functionally graded and multilayered materials (Pei and Asaro 1997, Carpinteri and Pugno 2006, Upadhyay and Simha 2007, Hsuesh *et al.* 2009, Her and Su 2015). The strain energy release rate is defined as

$$G = \frac{\Delta W_{ext} - \Delta U}{\Delta A_a}, \quad (2)$$

Where the change of external work, ΔW_{ext} , was expressed as

$$\Delta W_{ext} = \Delta U^* + \Delta U. \quad (3)$$

Here, ΔU^* and ΔU are the changes of complimentary strain energy and strain energy, respectively. By substitution of Eq. (2) in Eq. (3), we obtained

$$G = \frac{\Delta U^*}{\Delta A_a}, \quad (4)$$

Where

$$\Delta U^* = U_b^* - U_a^*. \quad (5)$$

Here, U_b^* and U_a^* are the complimentary strain energies before and after the increase of crack, respectively. The crack area increase, ΔA_a , was written as

$$\Delta A_a = 2\pi r \Delta a. \quad (6)$$

Thus, Eq. (4) was rewritten as

$$G = \frac{U_a^* - U_b^*}{2\pi r \Delta a}. \quad (7)$$

The complimentary strain energy before the crack increase was defined as

$$U_b^* = \iiint_{(V)} u_0^* dV, \quad (8)$$

Where (Fig. 2)

$$dV = 2\pi r_1 \Delta a dr_1, \quad 0 \leq r_1 \leq R. \quad (9)$$

The complimentary strain energy density, u_0^* , in Eq. (8) is equal to area OQS that supplement area OPQ enclosed by the stress-strain curve to a rectangle (Fig. 1). Therefore, the complimentary strain energy density was found as

$$u_0^* = \tau\gamma - \int_0^\gamma \tau(\gamma) d\gamma. \quad (10)$$

It should be specified that the material properties in the non-linear stress-strain relation, $\tau(\gamma)$, are functions of the radius, r_1 , where $0 \leq r_1 \leq R$, since the material of shaft is functionally graded in radial direction.

After integration in Eq. (10), γ should be replaced with

$$\gamma = r_1 \frac{\gamma_c}{R} \quad (11)$$

In order to facilitate the solution of integral Eq. (8). In Eq. (11), γ_c is the shear strain at the periphery of circular shaft cross-section. Relation Eq. (11) follows from the fact that according to the classical beam theory for torsion of circular shafts, the shear strains are distributed linearly along the radius of cross-section.

The strain γ_c in Eq. (11) should be found by considering the following equilibrium Equation

$$T = 2\pi \int_0^R \tau r_1^2 dr_1. \quad (12)$$

The integral in Eq. (12) should be solved for a particular stress-strain relation and then γ_c can be determined from the algebraic equation obtained.

In view of Eq. (9), the complimentary strain energy Eq. (8) was written as

$$U_b^* = 2\pi\Delta a \int_0^R u_0^* r_1 dr_1, \quad (13)$$

Where u_0^* is a function of r_1 via Eq. (11).

Eq. (13) can be used to determine the complimentary strain energy, $U_{a_1}^*$, in the internal crack arm after the crack increase. For this purpose, R and T should be replaced by r and T_1 , respectively (Fig. 4) in Eqs. (11), (12), and (13). Thus, the complimentary strain energy was written as

$$U_{a_1}^* = 2\pi\Delta a \int_0^r u_{0a_1}^* r_1 dr_1, \quad (14)$$

Where the complimentary strain energy density, $u_{0a_1}^*$, is a function of r , r_1 , and T_1 (after solution of Eq. (10), γ should be replaced by $\gamma=r_1 \gamma_c/r$, where γ_c is determined from Eq. (12) after replacing of R and T with r and T_1 , respectively).

In order to calculate the complimentary strain energy in the external crack arm, $U_{a_2}^*$, Eq. (13) was modified as

$$U_{a_2}^* = 2\pi\Delta a \int_r^R u_{0a_2}^* r_1 dr_1, \quad (15)$$

Where γ_c that participates in the complimentary strain energy density, $u_{0a_2}^*$, was obtained from the equilibrium equation

$$T_2 = 2\pi \int_r^R \tau r_1^2 dr_1. \quad (16)$$

Here, the torsion moment, T_2 , in the external crack arm behind the crack front was expressed by T and T_1 as

$$T_2 = T - T_1. \quad (17)$$

After integration in Eq. (16) for a particular stress-strain relation, the equation obtained can be solved with respect to γ_c .

The complimentary strain energy after the crack increase, U_a^* , was found by summation of Eqs. (14) and (15), i.e.,

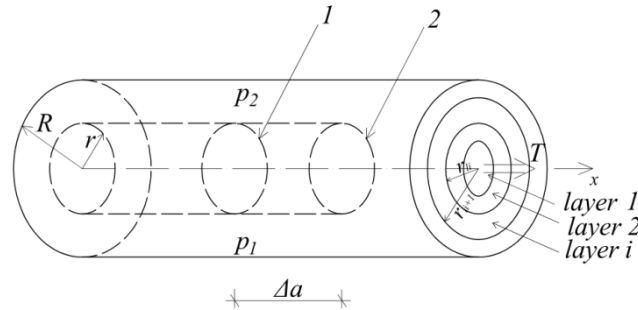


Fig. 5 Multilayered circular shaft portion with the crack front (1-crack front position before the increase of crack, 2-crack front position after the increase of crack). The longitudinal crack represents a cylindrical surface of radius r

$$U_a^* = U_{a_1}^* + U_{a_2}^* = 2\pi\Delta a \int_0^r u_{0a_1}^* r_1 dr_1 + 2\pi\Delta a \int_r^R u_{0a_2}^* r_1 dr_1. \quad (18)$$

The final solution was found after substitution of Eq. (13) and Eq. (18) in Eq. (5), i.e.,

$$G = \frac{1}{r} \left(\int_0^r u_{0a_1}^* r_1 dr_1 + \int_r^R u_{0a_2}^* r_1 dr_1 - \int_0^R u_0^* r_1 dr_1 \right). \quad (19)$$

Eq. (19) indicates that the strain energy release rate can be determined with taking into account the material non-linearity by using the torsion moments in the shaft cross-sections behind and ahead of the crack front only (the complimentary strain energy densities in Eq. (19) are functions of the cross-sectional torsion moments behind and ahead of the crack front).

It is obvious that Eq. (19) can also be applied to calculate the non-linear G in homogeneous shafts, i.e., shafts made by material that is not functionally graded. The only peculiarity is in solution of integrals, since the material properties are not functions of r_1 .

Non-linear fracture was analyzed also assuming that the shaft is made by multilayered materials as illustrated in Fig. 5. A longitudinal (interface) crack representing a cylindrical surface is located arbitrary between radial layers. The mechanical response of each layer is characterized by a non-linear stress-strain curve. The non-linear stress-strain relations were written as

$$\tau_i = \tau_i(\gamma), \quad i = 1, 2, \dots, n, \quad (20)$$

Where n is the layers number. The material constants in Eq. (20) may be different in each layer. Besides, different stress-strain relations may be used for each layer.

The strain energy release rate can be calculated by Eq. (5).

The complimentary strain energy before crack increase was written as

$$U_b^* = \sum_{i=1}^{i=n} \iiint_{(V_i)} u_{0i}^* dV_i, \quad (21)$$

Where dV_i can be found by Eq. (7) at $r_{li} \leq r_1 \leq r_{li+1}$ (refer to Fig. 5).

The complimentary strain energy density in each layer was obtained as

$$u_{0i}^* = \tau\gamma - \int_0^\gamma \tau_i(\gamma) d\gamma, i = 1, 2, \dots, n. \quad (22)$$

The strain γ_c (refer to Eq. (11)) should be determined by considering the following equilibrium equation of the multilayered shaft

$$T = \sum_{i=1}^{i=n} 2\pi \int_{r_i}^{r_{i+1}} \tau_i r_1^2 dr_1. \quad (23)$$

After solution of the integrals in Eq. (23), γ_c can be determined from the algebraic equation obtained. Then, after solution of integrals Eq. (22), γ should be replaced by Eq. (11). In this way, the strain energy density in each layer is obtained in function of r_1 to facilitate integration of Eq. (21).

In view of Eq. (9), the complimentary strain energy Eq. (21) was written as

$$U_b^* = 2\pi\Delta a \sum_{i=1}^{i=n} \int_{r_i}^{r_{i+1}} u_{0i}^* r_1 dr_1. \quad (24)$$

In order to determine the complimentary strain energy, $U_{a_1}^*$, in the internal crack arm after the increase of crack, Eq. (24) was modified in the following way

$$U_{a_1}^* = 2\pi\Delta a \sum_{i=1}^{i=n_1} \int_{r_i}^{r_{i+1}} u_{0a_1i}^* r_1 dr_1, \quad (25)$$

Where n_1 is the layers number in the internal crack arm. The complimentary strain energy density, $u_{0a_1i}^*$, can be obtained in a function of r , r_1 , and T_1 . For this purpose, R , T , and n should be replaced by r , T_1 , and n_1 , respectively in Eqs. (11), (22), and (23).

The complimentary strain energy in the external crack arm, $U_{a_2}^*$, was obtained by modifying Eq. (25) in the following way

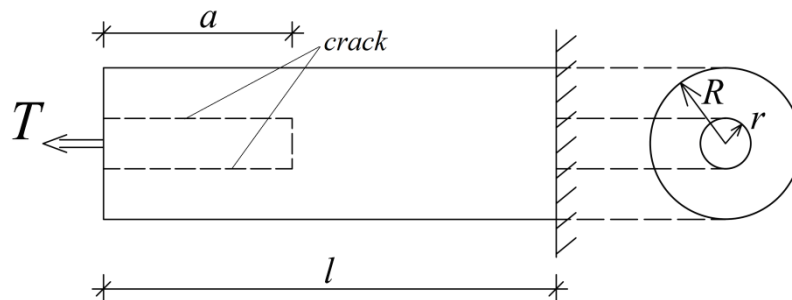
$$U_{a_2}^* = 2\pi\Delta a \sum_{i=1}^{i=n_2} \int_{r_i}^{r_{i+1}} u_{0a_2i}^* r_1 dr_1, \quad (26)$$

Where n_2 is the layers number in the external crack arm. The strain γ_c that participates in the complimentary strain energy density, $u_{0a_2i}^*$, was obtained from the equilibrium equation of external crack arm cross-section Eq. (16). For this purpose, Eq. (16) was modified as

$$T_2 = 2\pi \sum_{i=1}^{i=n_2} \int_{r_i}^{r_{i+1}} \tau r_1^2 dr_1, \quad (27)$$

Where T_2 was obtained by Eq. (15).

Finally, Eqs. (24), (25), and (26) were substituted in Eq. (5)

Fig. 6 Clamped circular shaft with longitudinal crack of length a

$$G = \frac{1}{r} \left(\sum_{i=1}^{i=n_1} \int_{r_i}^{r_{i+1}} u_{0a_1}^* r_1 dr_1 + \sum_{i=1}^{i=n_2} \int_{r_i}^{r_{i+1}} u_{0a_2}^* r_1 dr_1 - \sum_{i=1}^{i=n} \int_{r_i}^{r_{i+1}} u_{0i}^* r_1 dr_1 \right). \quad (28)$$

In this way, the non-linear fracture analysis of multilayered shafts loaded in torsion can be carried-out by using torsion moments in cross-sections behind and ahead of the crack front.

It should be mentioned that Eq. (28) can also be applied for non-linear analyses of the strain energy release rate in multilayered shafts made by functionally graded materials (material properties are functionally graded in radial direction). Besides, the type of gradation can be different in each layer. The only peculiarity is in solution of integrals, since the material properties are functions of r_1 .

3. Elastic-plastic investigation of fracture in a clamped shaft

The general non-linear fracture analyses of circular shafts in torsion developed in section 2 of the present paper were applied to investigate the strain energy release rate in the shaft shown in Fig. 6. There is a longitudinal crack of length a in the shaft. The radius of the internal crack arm is r . The shaft is clamped at its right-hand end. The loading consists of a torsion moment, T , applied at the free end of the internal crack arm. Therefore, the external crack arm is stress free.

First, the fracture was analyzed assuming that the shaft is homogeneous. Also, it was assumed that the mechanical behavior of shaft can be modeled by using a power law stress-strain relation (Petrov 2014)

$$\tau = H_s \gamma^{n_s}, \quad (29)$$

Where H_s and n_s are material properties.

The complimentary strain energy density was obtained by substitution of Eq. (29) in Eq. (10) and solving the integral

$$u_0^* = \frac{n_s H_s \gamma^{n_s+1}}{n_s + 1}. \quad (30)$$

The strain γ_c was determined from Eq. (12). For this purpose, Eqs. (11) and (29) were substituted in Eq. (12) and the integral was solved

$$T = \frac{2\pi R^3 H_s \gamma_c^{n_s}}{n_s + 3}. \quad (31)$$

From Eq. (31), we obtained

$$\gamma_c = \left[\frac{T(n_s + 3)}{2\pi R^3 H_s} \right]^{\frac{1}{n_s}}. \quad (32)$$

Eqs. (11) and (32) were substituted in Eq. (30), i.e.,

$$u_0^* = \frac{n_s H_s \left\{ \frac{r_1}{R} \left[\frac{T(n_s + 3)}{2\pi R^3 H_s} \right]^{\frac{1}{n_s}} \right\}^{n_s+1}}{n_s + 1}. \quad (33)$$

Eq. (33) expresses the complimentary strain energy density in the cross-section ahead of the crack front.

Radius, R , was replaced with r in Eq. (33) in order to determine the complimentary strain energy density in the internal crack arm

$$u_{0a_1}^* = \frac{n_s H_s \left\{ \frac{r_1}{r} \left[\frac{T(n_s + 3)}{2\pi r^3 H_s} \right]^{\frac{1}{n_s}} \right\}^{n_s+1}}{n_s + 1}. \quad (34)$$

In Eq. (34), it was taken into account that the torsion moment in the internal crack arm is T (Fig. 6).

The complimentary strain energy in the external crack arm is zero, since the latter is free of stresses (Fig. 6)

$$u_{0a_2}^* = 0. \quad (35)$$

Finally, Eqs. (33), (34) and (35) were substituted in Eq. (19) and the integrals were solved. It was obtained

$$G = \frac{1}{r} \left\{ \frac{n_s H_s \left\{ \frac{1}{r} \left[\frac{T(n_s + 3)}{2\pi r^3 H_s} \right]^{\frac{1}{n_s}} \right\}^{n_s+1} r^{n_s+3}}{(n_s + 1)(n_s + 3)} - \frac{n_s H_s \left\{ \frac{1}{R} \left[\frac{T(n_s + 3)}{2\pi R^3 H_s} \right]^{\frac{1}{n_s}} \right\}^{n_s+1} R^{n_s+3}}{(n_s + 1)(n_s + 3)} \right\}. \quad (36)$$

Obviously, at $n_s=1$, the power law stress-strain relation Eq. (29) transforms into the Hooke's law (assuming that the shear modulus is H_s). This means that at $n_s=1$ Eq. (36) should transform in

the formula for strain energy release rate in linear-elastic shaft. Indeed, by substitution of $n_s=1$ in Eq. (36), we found

$$G = \frac{T^2}{2\pi^2 r^5} \frac{R^4 - r^4}{H_s R^4}. \quad (37)$$

Which coincides with the formula for strain energy release rate derived by Rizov and Mladensky (2012) for linear-elastic homogeneous shaft.

In order to verify the non-linear solution Eq. (36), the strain energy release rate was determined also by considering the shaft complimentary strain energy. For this purpose, an elementary increase of the crack area, dA_a , was assumed leading to the following expression of strain energy release rate

$$G = \frac{dW_{ext} - dU}{dA_a}, \quad (38)$$

Where dW_{ext} and dU are the changes of external work and strain energy, respectively. The change of external work was expressed as

$$dW_{ext} = dU^* + dU, \quad (39)$$

Where dU^* is the change of complimentary strain energy. By combining of Eqs. (38) and (39), we derived

$$G = \frac{dU^*}{dA_a}, \quad (40)$$

Where

$$dA_a = 2\pi r da. \quad (41)$$

Here, da is an elementary crack increase. The complimentary strain energy density was integrated in the shaft volume in order to obtain the complimentary strain energy

$$U^* = \int_0^r u_{0a_1}^* 2\pi r_1 a dr_1 + \int_0^R u_0^* 2\pi r_1 (l-a) dr_1. \quad (42)$$

By combining of Eqs. (33), (34), (40), (41) and (42), we derived a formula that is exact match of Eq. (36). This fact is a verification of Eq. (36). Obviously, for the shaft configuration shown in Fig. 6, the strain energy release rate can be calculated relatively simply by using Eq. (40). However, for more complicated materials and loading conditions, Eq. (19) has decisive advantages over Eq. (40). For instance, one can calculate the strain energy release rate by Eq. (19) without analyzing the whole shaft (it is enough to analyze the stress state in the cross-sections ahead and behind the crack front only).

The fracture was analyzed also assuming that the material of shaft is functionally graded in radial direction. The mechanical behavior was modeled again by Eq. (29). The material property, H_s , was assumed to vary linearly as

$$H_s = H_{s0} + \frac{H_{s1} - H_{s0}}{R} r_1. \quad (43)$$

Where H_{s0} and H_{s1} are the values in the centre and at the periphery of the shaft cross-section. The strain γ_c was determined from the equilibrium Eq. (12), which was written as

$$T = \int_0^R 2\pi r_1^2 \left[H_{s0} + \frac{r_1}{R} (H_{s1} - H_{s0}) \right] \frac{r_1^{n_s}}{R^{n_s}} \gamma_c^{n_s} dr_1. \quad (44)$$

After performing the integration in Eq. (44) and solving the equation, γ_c was obtained as

$$\gamma_c = \left[\frac{T(n_s + 3)(n_s + 4)}{2\pi R^3 [H_{s0} + H_{s1}(n_s + 3)]} \right]^{\frac{1}{n_s}}. \quad (45)$$

It should be noted that at $H_{s0}=H_{s1}=H_s$, Eq. (45) transforms in Eq. (32).

The complimentary strain energy density was obtained by substitution of Eqs. (11), (43) and (45) in Eq. (30)

$$u_0^* = \frac{n_s \left[H_{s0} + \frac{H_{s1} - H_{s0}}{R} r_1 \right] \left\{ \frac{r_1}{R} \left[\frac{T(n_s + 3)(n_s + 4)}{2\pi R^3 [H_{s0} + H_{s1}(n_s + 3)]} \right]^{\frac{1}{n_s}} \right\}^{n_s + 1}}{n_s + 1}. \quad (46)$$

Obviously, at $H_{s0}=H_{s1}=H_s$, Eq. (46) transforms in Eq. (33).

Eq. (46) was used also to determine $u_{0a_1}^*$. For this purpose, R was replaced with r

$$u_{0a_1}^* = \frac{n_s \left[H_{s0} + \frac{H_{s1l} - H_{s0}}{r} r_1 \right] \left\{ \frac{r_1}{r} \left[\frac{T(n_s + 3)(n_s + 4)}{2\pi r^3 [H_{s0} + H_{s1l}(n_s + 3)]} \right]^{\frac{1}{n_s}} \right\}^{n_s + 1}}{n_s + 1}, \quad (47)$$

Where H_{s1l} is the value of H_s at the boundary between the internal and external crack arm. By using Eq. (43), H_{s1l} was written as

$$H_{s1l} = H_{s0} + \frac{H_{s1} - H_{s0}}{R} r. \quad (48)$$

It was mentioned above that the strain energy density in the external crack arm is zero.

The strain energy release rate was obtained by substitution of Eqs. (33), (44) and (47) in Eq. (19) and solving the integrals. The result is

$$H_{sl} = H_{s0} + \frac{H_{s1} - H_{s0}}{R} r. \quad (48)$$

$$G = \frac{1}{r} \left\{ \frac{n_s r^2}{n_s + 1} \left[\frac{H_{s0}}{n_s + 3} + \frac{H_{s1l} - H_{s0}}{n_s + 4} \right] \left[\frac{T(n_s + 3)(n_s + 4)}{2\pi r^3 [H_{s0} + H_{s1l}(n_s + 3)]} \right]^{\frac{n_s + 1}{n_s}} - \frac{n_s R^2}{n_s + 1} \left[\frac{H_{s0}}{n_s + 3} + \frac{H_{s1} - H_{s0}}{n_s + 4} \right] \left[\frac{T(n_s + 3)(n_s + 4)}{2\pi R^3 [H_{s0} + H_{s1}(n_s + 3)]} \right]^{\frac{n_s + 1}{n_s}} \right\}. \quad (49)$$

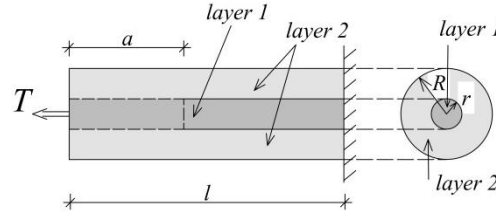


Fig. 7 Clamped bi-layer circular shaft with longitudinal crack of length a

It should be mentioned that at $H_{s0}=H_{s1}=H_s$, Eq. (49) transforms in Eq. (36).

Eq. (49) was verified by calculating of G with the help of Eq. (45). By substitution of Eqs. (41), (42), (46) and (47) in Eq. (45), we derived an expression that is exact match of Eq. (49). This fact verifies Eq. (49).

Non-linear fracture analysis was performed also for the bi-layer shaft shown in Fig. 7. There is a longitudinal crack of length, a , between the layers.

The internal layer 1 is a solid shaft with circular cross-section of radius r . It was assumed that the mechanical response of the internal layer can be modeled by stress-strain relation Eq. (29).

The mechanical behavior of the external layer 2 was modeled by using the following power-law stress-strain relation

$$\tau = Q_s \gamma^{n_q}, \quad (50)$$

Where Q_s and n_q are material properties.

The two layers were homogeneous. Besides, perfect adhesion was assumed between the layers in the un-cracked shaft portion.

The complimentary strain energy densities in the layers ahead and behind the crack front were needed in order to determine the strain energy release rate by Eq. (28). It should be noted that for the bi-layer shaft, $n_1=1$, $n_2=1$, $n_3=2$ (refer to Eq. (28)).

The strain γ_c at the periphery of the shaft cross-section ahead of the crack front was obtained from the equilibrium Eq. (23). For this purpose, Eq. (23) was rewritten as

$$T = 2\pi \int_0^r H_s \gamma^{n_s} r_1^2 dr_1 + 2\pi \int_r^R Q_s \gamma^{n_q} r_1^2 dr_1. \quad (51)$$

After substitution of Eq. (11) in Eq. (51) and solving the integrals, it was obtained

$$T = \frac{2\pi r^{n_s+3} H_s \gamma_c^{n_s}}{R^{n_s} (n_s + 3)} + \frac{2\pi Q_s \gamma_c^{n_q} (R^{n_q+3} - r^{n_q+3})}{R^{n_q} (n_q + 3)}. \quad (52)$$

Eq. (52) should be solved with respect to γ_c by using the MatLab computer program.

The complimentary strain energy density in the internal layer 1 (Fig. 7) was obtained by substitution of Eq. (11) in Eq. (30)

$$u_{01}^* = \frac{n_s H_s \left(r_1 \frac{\gamma_c}{R} \right)^{n_s+1}}{n_s + 1}, \quad 0 \leq r_1 \leq r. \quad (53)$$

Eq. (53) was used also to determine the complimentary strain energy density in the external layer 2 in the un-cracked shaft portion (ahead of the crack front). For this purpose, n_s and \underline{H}_s were replaced with n_q and Q_s , respectively

$$u_{02}^* = \frac{n_q Q_s \left(r_1 \frac{\gamma_c}{R} \right)^{n_q+1}}{n_q + 1}, \quad r \leq r_1 \leq R. \quad (54)$$

The strain energy density in the internal crack arm behind the crack front, u_{0a1} , was found by Eq. (34).

After substitution of Eqs. (34), (35), (53) and (54) in Eq. (19) and solving the integrals, the strain energy release rate was written as

$$G = \frac{1}{r} \left\{ \frac{n_s H_s \left\{ \frac{1}{r} \left[\frac{T(n_s+3)}{2\pi r^3 H_s} \right]^{n_s} \right\}^{n_s+1} r^{n_s+3}}{(n_s+1)(n_s+3)} - \frac{n_s H_s \gamma_c^{n_s+1} r^{n_s+3}}{R^{n_s+1} (n_s+1)(n_s+3)} - \frac{n_q Q_s \gamma_c^{n_q+1} (R^{n_q+3} - r^{n_q+3})}{R^{n_q+1} (n_q+1)(n_q+3)} \right\}, \quad (55)$$

Where γ_c was determined from Eq. (52).

It is clear that at $n_s=1$ and $n_q=1$, the stress-strain relations Eqs. (29) and (49) transform in the Hooke's law (assuming that H_s and Q_s are the shear moduli of internal and external layer, respectively). Indeed, by substitution of $n_s=1$ and $n_q=1$ in Eq. (55), we obtained

$$G = \frac{T}{2\pi^2 r^5} \frac{Q_s (R^4 - r^4)}{H_s (H_s - Q_s) r^4 + H_s Q_s R^4}, \quad (56)$$

Which coincides with the formula for strain energy release rate in the linear-elastic bi-layer shaft (Rizov and Mladensky 2012).

The strain energy release rate in the bi-layer shaft shown in Fig. 7 was determined also by Eq. (40) in order to verify Eq. (55). For this purpose, the complimentary strain energy was written as

$$U^* = \int_0^r u_{0a1}^* 2\pi r_1 a dr_1 + \int_0^r u_{01}^* 2\pi r_1 (l-a) dr_1 + \int_r^R u_{02}^* 2\pi r_1 (l-a) dr_1. \quad (57)$$

By substitution of Eqs. (34), (41), (53), (54) and (57) in Eq. (40), we derived a formula that is exact match of Eq. (55). This fact is verification of Eq. (55).

The non-linear fracture in the bi-layer shaft (Fig. 7) was studied also assuming that the material is functionally graded in radial direction. The mechanical behavior of the internal and external layer was modeled by stress-strain relations Eqs. (29) and (50), respectively.

For the material in the internal layer, it was assumed that H_s (refer to Eq. (29)) varies non-linearly along the shaft cross-section radius

$$H_s = H_{s0} + (H_{s1} - H_{s0}) \frac{r_1^m}{r^m}, \quad 0 \leq r_1 \leq r, \quad (58)$$

Where H_{s0} and H_{s1} are the values of H_s in the centre and in the boundary between the two layers, respectively, m is a non-dimensional parameter.

In the external layer, it was assumed that Q_s (refer to Eq. (60)) varies linearly in radial direction

$$Q_s = Q_{s0} + \frac{Q_{s1} - Q_{s0}}{R - r} (r_1 - r), \quad r \leq r_1 \leq R, \quad (59)$$

Where Q_{s0} and Q_{s1} are the values of Q_s in the boundary between the two layers and at the periphery of shaft, respectively.

The strain, γ_c , at the periphery of shaft cross-section was determined from the equilibrium Eq. (21). After substitution of Eqs. (11), (29), (50), (58) and (59) in Eq. (23), it was found

$$T = 2\pi\gamma_c^n r^3 \frac{H_{s1}(n_s + 3) + H_{s0}m}{(n_s + 3)(n_s + m + 3)} + \frac{2\pi\gamma_c^{n_q} (R^{n_q+3} - r^{n_q+3})}{R^{n_q} (n_q + 3)} \left(Q_{s0} - \frac{Q_{s1} - Q_{s0}}{R - r} r \right) + \frac{2\pi\gamma_c^{n_q} (Q_{s1} - Q_{s0}) (R^{n_q+4} - r^{n_q+4})}{R^{n_q} (R - r) (n_q + 4)}. \quad (60)$$

It should be noted that at $H_{s0}=H_{s1}=H_s$ and $Q_{s0}=Q_{s1}=Q_s$, Eq. (60) transforms in Eq. (52).

Eq. (60) should be solved with respect to γ_c by using the MatLab computer program.

Eq. (53) was applied to determine the complimentary strain energy density, u_{01}^* , in the internal layer 1. For this purpose, Eq. (58) was substituted in Eq. (53)

$$u_{01}^* = \frac{n_s \left[H_{s0} + (H_{s1} - H_{s0}) \frac{r_1^m}{r^m} \right] \left(r_1 \frac{\gamma_c}{R} \right)^{n_s+1}}{n_s + 1}, \quad 0 \leq r_1 \leq r. \quad (61)$$

Eq. (59) was substituted in Eq. (53) to obtain the complimentary strain energy density, u_{02}^* , in the external layer 2

$$u_{02}^* = \frac{n_q \left[Q_{s0} + \frac{Q_{s1} - Q_{s0}}{R - r} (r_1 - r) \right] \left(r_1 \frac{\gamma_c}{R} \right)^{n_q+1}}{n_q + 1}, \quad r \leq r_1 \leq R. \quad (62)$$

The strain energy density in the internal crack arm behind the crack front, u_{0a1}^* , was obtained in the following way. In order to determine the strain at the periphery of the internal crack arm, γ_{cl} , Eqs. (29) and (52) were substituted in the equilibrium Eq. (12), R was replaced with r and the integral was solved

$$T = 2\pi\gamma_{cl}^{n_s} r^3 \frac{H_{s1}(n_s + 3) + H_{s0}m}{(n_s + 3)(n_s + m + 3)}. \quad (63)$$

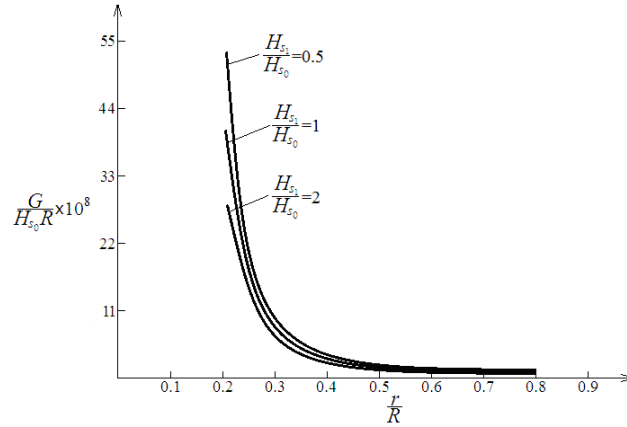


Fig. 8 The strain energy release rate in non-dimensional form plotted against r/R ratio at $H_{s1}/H_{s0}=0.5, 1$ and 2 for the functionally graded shaft shown in Fig. 6

From Eq. (63), it was found

$$\gamma_{cl} = \left\{ \frac{T(n_s + 3)(n_s + m + 3)}{2\pi r^3 [H_{s1}(n_s + 3) + H_{s0}m]} \right\}^{\frac{1}{n_s}} \quad (64)$$

Eq. (61) was used to determine u_{0a1}^* . For this purpose, R and γ_c were replaced with r and γ_{cl} , respectively

$$u_{0a1}^* = \frac{n_s \left[H_{s0} + (H_{s1} - H_{s0}) \frac{r_1^m}{r^m} \right] \left(\frac{r_1}{r} \right)^{n_s+1}}{n_s + 1} \left\{ \frac{T(n_s + 3)(n_s + m + 3)}{2\pi r^3 [H_{s1}(n_s + 3) + H_{s0}m]} \right\}^{\frac{n_s+1}{n_s}}, \quad 0 \leq r_1 \leq r. \quad (65)$$

After substitution of Eqs. (35), (61), (62) and (65) in Eq. (28) and solving the integrals, the strain energy release rate was written as

$$G = \frac{1}{r} \left\{ \frac{n_s r^2 [H_{s0}m + H_{s1}(n_s + 3)]}{(n_s + 1)(n_s + 3)(m + n_s + 3)} \left\{ \frac{T(n_s + 3)(n_s + m + 3)}{2\pi r^3 [H_{s1}(n_s + 3) + H_{s0}m]} \right\}^{\frac{n_s+1}{n_s}} - \frac{n_s [H_{s0}m + H_{s1}(n_s + 3)] r^{n_s+3} \left(\frac{\gamma_c}{R} \right)^{n_s+1}}{(n_s + 1)(n_s + 3)(m + n_s + 3)} - \frac{n_q \gamma_c^{n_q+1}}{R^{n_q+1} (n_q + 1)} \left[\frac{Q_{s0} (R^{n_q+3} - r^{n_q+3})}{n_q + 3} + \frac{Q_{s1} - Q_{s0}}{R - r} \left(\frac{R^{n_q+4} - r^{n_q+4}}{n_q + 4} - r \frac{R^{n_q+3} - r^{n_q+3}}{n_q + 3} \right) \right] \right\}, \quad (66)$$

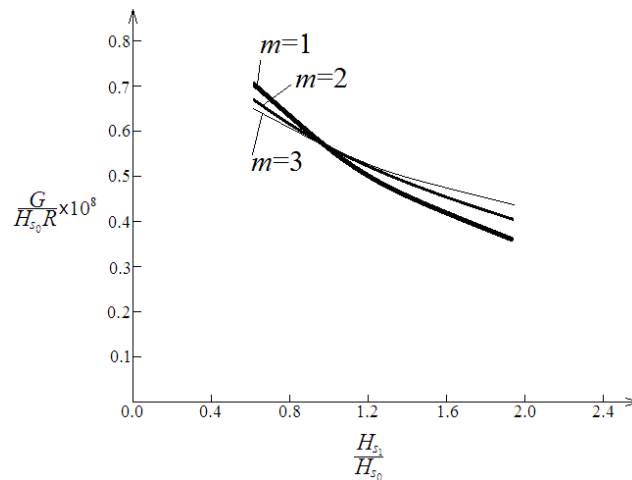


Fig. 9 The strain energy release rate in non-dimensional form plotted against H_{s1}/H_{s0} ratio at $m=1, 2$ and 3 for the functionally graded bi-layer shaft shown in Fig. 7

Where γ_c should be determined from Eq. (60). It should be noted that at $H_{s0}=H_{s1}=H_s$ and $Q_{s0}=Q_{s1}=Q_s$, Eq. (66) transforms in Eq. (55).

In order to verify Eq. (64), the strain energy release rate was determined by Eq. (40). By substitution Eqs. (41), (57), (61), (62) and (65) in Eq. (40), we obtained a formula that is exact match of Eq. (66). This fact is a verification of Eq. (66).

4. Parametric investigations

Parametric investigations were carried-out of elastic-plastic fracture in the clamped circular shafts shown in Fig. 6 and Fig. 7. In these investigations, the crack location along the shaft cross-section was characterized by r/R ratio.

First, the influence was analyzed of material properties and crack location on the non-linear fracture behavior of functionally graded circular shaft shown in Fig. 6. For this purpose, the strain energy release rate was calculated by using Eq. (49). In these calculations, it was assumed that $T=10$ Nm and $R=0.02$ m. The strain energy release rate calculated was presented in non-dimensional form by using the formula $G_N=G/(H_{s0}R)$. The results of calculations are illustrated in Fig. 8, where the strain energy release rate is plotted against r/R ratio at $H_{s1}/H_{s0}=0.5, 1$ and 2. The diagrams in Fig. 8 indicate that the strain energy release rate decreases with increasing r/R ratio. This finding was attributed to increase of the stiffness of internal crack arm (the external crack arm is free of stresses). Also, one can observe that increase of H_{s1}/H_{s0} ratio leads to decrease of the strain energy release rate (this is due to increase of the shaft stiffness).

For the functionally graded bi-layered circular shaft (Fig. 7), the strain energy release rate was calculated by Eq. (66) and plotted in non-dimensional form as a function of H_{s1}/H_{s0} ratio at $m=1, 2$ and 3 in Fig. 9 (the material properties H_{s1} , H_{s0} and m are defined in Eq. (58)). It was assumed also that $r/R=0.5$, $Q_{s0}/H_{s0}=0.6$ and $Q_{s1}/Q_{s0}=1.2$. It can be observed (Fig. 9) that in the functionally graded bi-layered circular shaft the strain energy release rate decreases with increasing H_{s1}/H_{s0} ratio (this was explained with increase of the shaft stiffness). The curves in Fig. 9 indicate also that

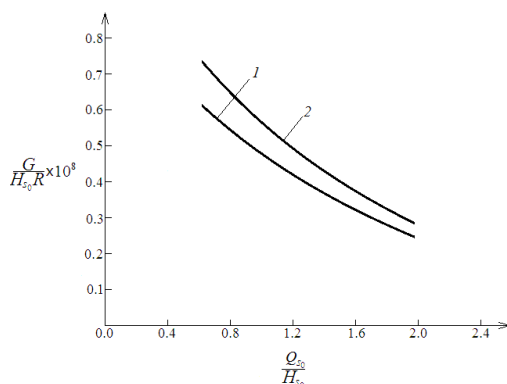


Fig. 10 The strain energy release rate in non-dimensional form plotted against Q_{s0}/H_{s0} ratio for the functionally graded bi-layer shaft (1-linear-elastic material behavior, 2-non-linear material behavior)

the strain energy release rate decreases with increase of m at $H_{s1}/H_{s0} < 1$. The increase of m leads to increase of the strain energy release rate, when $H_{s1}/H_{s0} > 1$.

The influence of Q_{s0}/H_{s0} ratio on the non-linear fracture behavior of functionally graded bi-layered circular shaft (Fig. 7) was analyzed too. For this purpose, the strain energy release rate was calculated by Eq. (66) and plotted against Q_{s0}/H_{s0} ratio in Fig. 10 (the calculations were performed assuming that $r/R=0.5$, $H_{s1}/H_{s0}=0.9$, $m=2$ and $Q_{s1}/Q_{s0}=1.3$). The results shown in Fig. 10 indicate that the strain energy release rate decreases with the increasing Q_{s0}/H_{s0} ratio. Also, the influence was analyzed of material non-linearity on the fracture behavior.

For this purpose, calculations were carried-out of the strain energy release rate assuming linear-elastic material behavior of the shaft (the linear-elastic solution was obtained by substitution of $n_s=n_q=1$ in Eq. (66)). The results of these calculations were plotted against Q_{s0}/H_{s0} ratio as shown in Fig. 10. It can be observed that the material non-linearity leads to increase of the strain energy release rate (Fig. 10). This finding indicates that the non-linear material behavior has to be taken into account in fracture mechanics based safety design of functionally graded and multilayered shafts in torsion.

5. Conclusions

Longitudinal fracture behavior of circular shafts in torsion was modeled analytically. The basic purpose was to develop a fracture analysis with considering the material non-linearity. The general expression was derived of strain energy release rate in a function of the torsion moments in the cross-sections ahead and behind the crack front. The mechanical response of shafts was described by non-linear relations between the shear stresses and shear strains. Fracture in functionally graded and multilayered shafts was analyzed. The analytical approach developed was applied to study the fracture behavior of a clamped circular shaft in torsion. In order to verify the non-linear solution derived, the strain energy release rate was determined also by considering the shaft complimentary strain energy. Different material gradients in radial direction were used in the fracture analysis. The influence of material properties, crack location and material non-linearity on the fracture behavior was investigated. The basic advantage of the analytical approach developed in the present paper is that the strain energy release rate can be calculated (with considering the material non-

linearity) by using the torsion moments in the cross-sections ahead and behind the crack front only. The analytical solution derived is very convenient for parametric investigations. The present study contributes for the understanding of longitudinal fracture in functionally graded multilayered circular shafts that exhibit material non-linearity.

Acknowledgments

The present study was supported financially by the Research and Design Centre (CNIP) of the UACEG, Sofia (Contract BN-189/2016).

References

- Abdelhak, Z., Hadji, L., Daouadji, T. and Bedia, E. (2015), "Thermal buckling of functionally graded plates using an-order four variable refined theory", *Adv. Mater. Res.*, **4**(1), 31-44.
- Ait, Y.S., Ait, A.H., Houari, M.S.A. and Tounsi, A. (2015), "Wave propagation in functionally graded plates with porosities using various higher-order shear deformation plate theories", *Struct. Eng. Mech.*, **53**(6), 1143-1165.
- Belabed, Z., Houari, M.S.A., Tounsi, A., Mahmoud, S.R. and Anwar, B.O. (2014), "An efficient and simple higher order shear and normal deformation theory for functionally graded material (FGM) plates", *Compos.: Part B*, **60**, 274-283.
- Bellifa, H., Benrahou, K.H., Hadji, L., Houari, M.S.A. and Tounsi, A. (2016), "Bending and free vibration analysis of functionally graded plates using a simple shear deformation theory and the concept the neutral surface position", *J. Brazil. Soc. Mech. Sci. Eng.*, **38**(1), 265-275.
- Bennoun, M., Houari, M.S.A. and Tounsi, A. (2016), "A novel five variable refined plate theory for vibration analysis of functionally graded sandwich plates", *Mech. Adv. Mater. Struct.*, **23**(4), 423-431.
- Bohidar, S.K., Sharma, R. and Mishra, P.R. (2014), "Functionally graded materials: A critical review", *J. Res.*, **1**(7), 289-301.
- Bouderba, B., Houari, M.S.A. and Tounsi, A. (2013), "Thermomechanical bending response of FGM thick plates resting on winkler-pasternak elastic foundations", *Steel Compos. Struct.*, **14**(1), 85-104.
- Bourada, F., Amara, K. and Tounsi, A. (2016), "Buckling analysis of isotropic and orthotropic plates using a novel four variable refined plate theory", *Steel Compos. Struct.*, **21**(6), 1287-1306.
- Bourada, M., Kaci, A., Houari, M.S.A. and Tounsi, A. (2015), "A new simple shear and normal deformations theory for functionally graded beams", *Steel Compos. Struct.*, **18**(2), 409-423.
- Bousahla, A.A., Houari, M.S.A., Tounsi, A. and Adda Bedia, E.A. (2014), "A novel higher order shear and normal deformation theory based on neutral surface position for bending analysis of advanced composite plates", *J. Comput. Methods*, **11**(6), 1350082.
- Carpinteri, A. and Pugno, N. (2006), "Cracks in re-entrant corners in functionally graded materials", *Eng. Fract. Mech.*, **73**(6), 1279-1291.
- Chakrabarty, J. (2006), *Theory of Plasticity*, Elsevier Butterworth-Heinemann, Oxford.
- Daouadji, T. and Adim, B. (2016), "Theoretical analysis of composite beams under uniformly distributed load", *Adv. Mater. Res.*, **5**(1), 1-9.
- Daouadji, T., Adim, B. and Benferhat, R. (2016), "Bending analysis of an imperfect FGM plates under hygro-thermo-mechanical loading with analytical validation", *Adv. Mater. Res.*, **5**(1), 35-53.
- Gasik, M.M. (2010), "Functionally graded materials: Bulk processing techniques", *J. Mater. Prod. Technol.*, **39**(1-2), 20-29.
- Guadette, F.G., Giannopoulos, A.E. and Suresh, S. (2001), "Interfacial cracks in layered materials subjected to a uniform temperature change", *J. Fract.*, **28**(1), 5620-5629.

- Hadji, L., Khelifa, Z. and Bedia, E.A.A. (2016), "A New higher order shear deformation model for functionally graded beams", *KSCE J. Civil Eng.*, **20**(5), 1835-1841.
- Hamidi, A., Houari, M.S.A., Mahmoud, S.R. and Tounsi, A. (2015), "A sinusoidal plate theory with 5-unknowns and stretching effect for thermomechanical bending of functionally graded sandwich plates", *Steel Compos. Struct.*, **18**(1), 235-253.
- Her, S.C. and Su, W.B. (2015), "Interfacial fracture toughness of multilayered composite structures", *Strength Mater.*, **47**(1), 186-191.
- Hsueh, C.H., Tuan, W.H. and Wei, W.C.J. (2009), "Analyses of steady-state interface fracture of elastic multilayered beams under four-point bending", *Scripta Mater.*, **60**(1), 721-724.
- Ivanov, I. and Draganov, I. (2014), "Influence and simulation of laminated glass subjected to low-velocity impact", *Mech. Mach.*, **110**, 89-94.
- Ivanov, V., Velchev, D.S., Georgiev, N.G., Ivanov, I.D. and Sadowski, T. (2016), "A plate finite element for modelling of triplex laminated glass and comparison with other computational models", *Meccanica*, **51**(2), 341-358.
- Jiao, J., Gurumurthy, G.K., Kramer, E.J., Sha, Y., Hui, C.Y. and Borgesen, P. (1998), "Measurement of interfacial fracture toughness under combined mechanical and thermal stress", *J. Electr. Pack.*, **120**(1), 325-349.
- Mahi, A., Bedia, E.A.A. and Tounsi, A. (2015), "A new hyperbolic shear deformation theory for bending and free vibration analysis of isotropic, functionally graded, sandwich and laminated composite plates", *Appl. Math. Model.*, **39**(9), 2489-2508.
- Markov, I. and Dinev, D. (2005), "Theoretical and experimental investigation of a beam strengthened by bonded composite strip", *Proceedings of the International Scientific Conference VSU*.
- Nemat-Allal, M.M., Ata, M.H., Bayoumi, M.R. and Khair-Eldeen, W. (2011), "Powder metallurgical fabrication and microstructural investigations of Aluminum/Steel functionally graded material", *Mater. Sci. Appl.*, **2**(5), 1708-1718.
- Pei, G. and Asaro, R.J. (1997), "Cracks in functionally graded materials", *J. Solids Struct.*, **34**(1), 1-17.
- Petrov, V.V. (2014), *Non-Linear Incremental Structural Mechanics*, M.: Infra-Injeneria.
- Rizov, V. and Mladensky, A. (2012), "Crack investigation in bi-layered composite beam of circular cross-section", *J. Mater. Sci. Technol.*, **20**(2), 72-83.
- Szekrenyes, A. and Vicente, W.M. (2012), "Interlaminar fracture analysis in the GII-GIII plane using prestressed transparent composite beams", *Compos. Part A: Appl. Sci. Manufact.*, **43**(1), 95-103.
- Szekrenyes, A. (2010), "Fracture analysis in the modified split-cantilever beam using the classical theories of strength of materials", *J. Phys. Conf. Series*, **240**(1), 012030.
- Tilbrook, M.T., Moon, R.J. and Hoffman, M. (2005), "Crack propagation in graded composites", *Compos. Sci. Technol.*, **65**(2), 201-220.
- Upadhyay, A.K. and Simha, K.R.Y. (2007), "Equivalent homogeneous variable depth beams for cracked FGM beams; compliance approach", *J. Fract.*, **144**(2), 209-213.
- Yeung, D.T.S., Lam, D.C.C. and Yuen, M.M.F. (2000), "Specimen design for mixed mode interfacial fracture properties measurement in electronic packages", *J. Electr. Pack.*, **122**(2), 67-72.
- Zhang, H., Li, X.F., Tang, G.J. and Shen, Z.B. (2013), "Stress intensity factors of double cantilever nanobeams via gradient elasticity theory", *Eng. Fract. Mech.*, **105**(1), 58-64.